02FCC-37

Impact of SiC Power Electronic Devices for Hybrid Electric Vehicles

Leon M. Tolbert[1,2], Burak Ozpineci[1,3], Syed K. Islam[1], Fang Z. Peng[2,4]
[1]The University of Tennessee
[2]Oak Ridge National Laboratory
[3]Oak Ridge Institute for Science and Education
[4]Michigan State University

ABSTRACT*

The superior properties of silicon carbide (SiC) power electronic devices compared with silicon (Si) are expected to have a significant impact on next-generation vehicles, especially hybrid electric vehicles (HEVs). The system-level benefits of using SiC devices in HEVs include a large reduction in the size, weight, and cost of the power conditioning and/or thermal systems. However, the expected performance characteristics of the various semiconductor devices and the impact that these devices could have in applications are not well understood. Simulation tools have been developed and are demonstrated for SiC devices in relevant transportation applications. These tools have been verified by experimental analysis of SiC diodes and MOSFETs and can be used to assess the impact of expected performance gains in SiC devices and determine areas of greatest impact in HEV systems.

INTRODUCTION

Presently, almost all of the power electronics converter systems in automotive applications use silicon- (Si-) based power semiconductor switches. The performance of these systems is approaching the theoretical limits of the Si fundamental material properties. The emergence of silicon carbide- (SiC-) based power semiconductor switches likely will result in substantial improvements in the performance of power electronics converter systems in transportation applications. SiC is a wide-bandgap semiconductor, and SiC-based power switches can be used in electric traction drives and other automotive electrical subsystems with many benefits compared with Si-based switches.

In this paper, experimental characteristics of Si and SiC are used to develop a simulation model for SiC power electronics devices. The main objective of developing these simulation tools is to show some of the system-level benefits of using SiC devices in HEVs such as the large reduction in the size, weight, and cost of the power conditioning and/or thermal management systems. Temperature-dependent circuit models for SiC diodes and MOSFETs have been developed. Power losses and device temperatures have been computed for a traction drive in HEVs. Temperature and efficiency profiles have been created for the devices for powering a vehicle over an urban driving cycle. The system benefits in using SiC devices are highlighted through simulation and experimental results.

At Oak Ridge National Laboratory (ORNL), a SiC power MOSFET is presently being designed. This power device will be used in power electronics converter systems for automotive applications to demonstrate the benefits of SiC-based power devices. One of the selected automotive applications for this project is a traction drive. New gate drive layouts, circuit topologies, and filter requirements will also be developed to take advantage of the special properties of SiC devices.

ADVANTAGES OF SiC COMPARED WITH Si

As mentioned earlier, SiC is a wide-bandgap semiconductor, and this property of SiC is expected to yield greatly superior power electronics devices once processing and fabrication issues with this material are solved. Some of the advantages of SiC compared with Si based power devices are as follows:

1. SiC-based power devices have higher breakdown voltages (5 to 30 times higher than those of Si) because of their higher electric breakdown field.

2. SiC devices are thinner, and they have lower on-resistances. The substantially higher breakdown-voltage for SiC allows higher concentrations of doping and consequently a lower series resistance. For low-breakdown voltage devices (~50V), SiC unipolar device on-resistances are around 100 times less; and at higher breakdown voltages (~5000V), they are up

*Prepared by the Oak Ridge National Laboratory, Oak Ridge, Tennessee 37831, managed by UT-Battelle for the U.S. Department of Energy under contract DE-AC05-00OR22725.

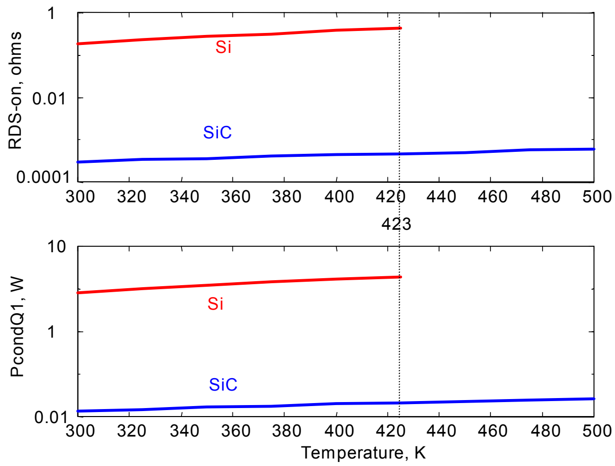

Figure 1. The change in MOSFET on-resistance and conduction losses with temperature. Note that Si cannot withstand temperatures of over 423K (150°C) (Si-red, 4H-SiC-blue, logarithmic y-axis).

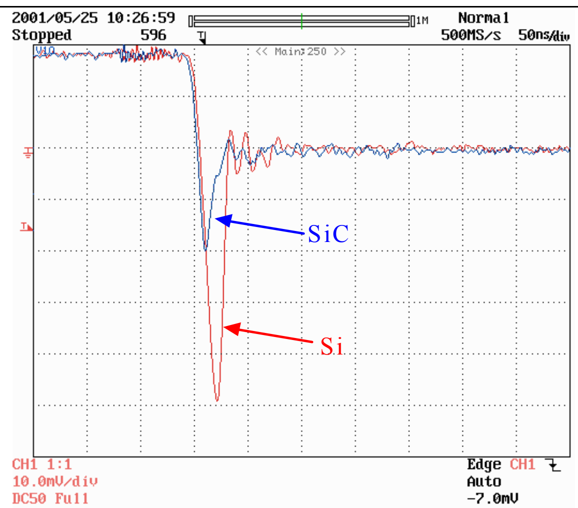

Figure 2. Typical experimental Si and SiC diode reverse recovery (2A/div).

to 300 times less [1]. With lower R_{on}, SiC unipolar power devices have lower conduction losses (Figure 1) and therefore higher overall efficiency.

3. SiC has a higher thermal conductivity and thus a lower junction-to-case thermal resistance, $R_{th\text{-}jc}$. This means heat is more easily conducted away from the device junction, and thus the device temperature increase is slower.

4. SiC can operate at high temperatures because of its wider bandgap. SiC device operation at up to 600°C is mentioned in the literature [2]. Most Si devices, on the other hand, can operate at a maximum junction temperature of only 150°C.

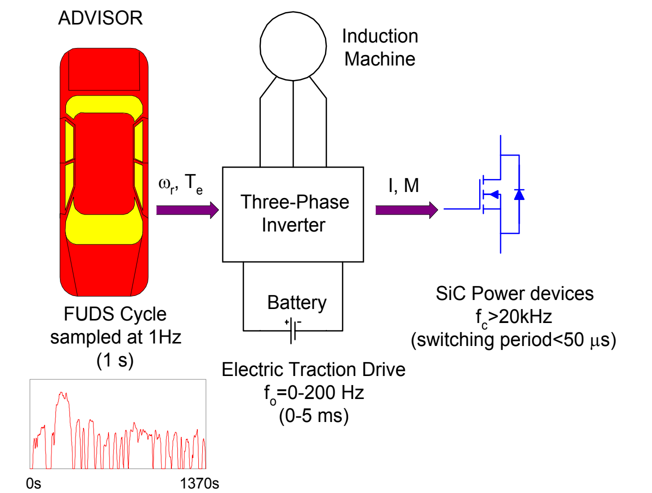

Figure 3. Block Diagram of the Model.

5. Forward and reverse characteristics of SiC power devices vary only slightly with temperature and time; therefore, SiC devices are more reliable.

6. SiC-based devices have excellent reverse recovery characteristics [3]. With less reverse recovery current, the switching losses and electromagnetic interference (EMI) are reduced and there is less or no need for snubbers. Typical turn-off waveforms of commercial Si and SiC diodes are given in Figure 2.

7. SiC is extremely radiation hard; i.e., radiation does not degrade the electronic properties of SiC.

MACHINE AND INVERTER MODELING

System level simulation tools have been developed to calculate the conduction and switching losses of the power devices in an inverter used as a motor drive in an HEV. The efficiency of the inverter can then be determined from these losses. The simulation tool is also able to estimate the junction temperature of the power semiconductor devices and recommend an appropriate heatsink size.

In this paper, an averaging technique [4] is used to model the power electronics switching losses in an HEV traction drive system. The models are compatible with the Department of Energy's <u>AD</u>vanced <u>V</u>eh<u>I</u>cle <u>S</u>imulat<u>OR</u> (ADVISOR) models. The developed system models use torque and speed values from the ADVISOR simulation to determine the current profile of the system over the Federal Urban Driving Schedule (FUDS). Circuit-level simulation is not practical for this work because the device variables are in micro- or nanoseconds and the system variables are in 1-second increments.

Figure 3 shows the block diagram of the system modeling approach, and Figure 4 shows the three-phase inverter and induction machine for the traction drive system.

The main losses on the power devices are conduction losses and switching losses. These losses will be calculated separately in the following subsections for diodes and MOSFETs in the three-phase pulse-width modulation (PWM) inverter.

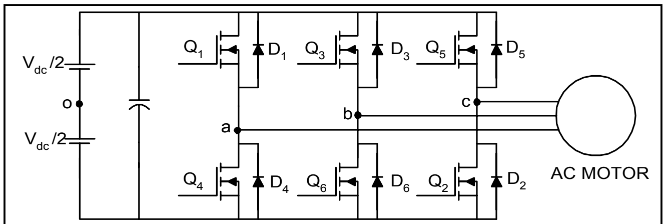

Figure 4. Three-phase inverter driving an induction machine load.

LOSS MODELING FOR MOSFETS

CONDUCTION LOSSES:

Conduction losses of a MOSFET Q_1 are given by

$$P_{cond,Q1} = I^2_{Q1,rms} \cdot R_{DS,on} \,. \qquad (1)$$

$I_{Q1,rms}$ in a three-phase PWM inverter, can be found directly by

$$I_{Q1,rms} = \sqrt{\frac{1}{N}\sum_{n=0}^{N-1} i^2_{o,n} D_n} = I\sqrt{\frac{1}{8}+\frac{1}{3\pi}M\cos\phi} \qquad (2)$$

where D_n = duty ratio in the nth interval,

$i_{o,n}$ = average output current in the nth interval,

$$N = \frac{f_c}{f_o} = \frac{T_o}{T_c} \,. \qquad (3)$$

$i_{o,n} = I\sin(\theta_n - \phi)$, I = peak output current. (4)

$\theta_n = \frac{2\pi\, n}{N}$, ϕ = phase angle of the current. (5)

$D_n = \frac{1}{2}\left(1 + M\sin\theta_n\right)$ (duty ratio of a switch in a sinusoidal PWM inverter). (6)

Thus

$$P_{cond,Q1} = I^2 \cdot R_{DS,on} \cdot \left(\frac{1}{8}+\frac{1}{3\pi}M\cos\phi\right). \qquad (7)$$

SWITCHING LOSSES:

Most switching loss calculations reported in the literature use an approximate linear model for device turn-on and turn-off. This practice does not consider the device physics. In this paper, on the other hand, physics-based energy loss equations from Huang and Zhang [5] will be considered to calculate the MOSFET switching losses. Energy loss during switching in a MOSFET is expressed as follows:

$$\begin{aligned} E_{tot} &= E_{on} + E_{off} \\ &= \frac{1}{3(K_1-1)}\varepsilon_s E_c V\left(\frac{V}{BV}\right)^{1/2} + \frac{1}{3(K_2+1)}\varepsilon_s E_c V\left(\frac{V}{BV}\right)^{1/2} \qquad (8) \\ &= D\left(\frac{J}{C_1-J}+\frac{J}{C_2+J}\right) \end{aligned}$$

where $K_1 = \frac{g_m(V_{GH}-V_{th})}{J}$, $K_2 = \frac{g_m(V_{th}-V_{GL})}{J}$,

$D = \frac{1}{3}\varepsilon_s E_c V\left(\frac{V}{BV}\right)^{1/2}$, $C_1 = g_m(V_{GH}-V_{th})$,

$C_2 = g_m(V_{th}-V_{GL})$,

and $J = \frac{I}{A}\sin(\theta-\phi) = J'\sin(\theta-\phi)$

Q_1 switching loss in one switching period, T_c, is

$$p_{Q1} = \frac{E_{on}+E_{off}}{T_c} = f_c E_{tot} \qquad (9)$$

Averaging over the output period, T_o,

$$P_{sw,Q1} = \frac{Df_c}{2\pi}\left[\frac{C_1}{\sqrt{C_1^2-J'^2}}\left(\pi + 2\tan^{-1}\left(\frac{J'}{\sqrt{C_1^2-J'^2}}\right)\right) + \frac{C_2}{\sqrt{C_2^2-J'^2}}\left(-\pi + 2\tan^{-1}\left(\frac{J'}{\sqrt{C_2^2-J'^2}}\right)\right)\right]. \qquad (10)$$

Note that all six MOSFETs have the same switching and conduction losses for a balanced three-phase load. To find the total MOSFET losses of the inverter, $P_{cond,\,Q1}$ and $P_{sw,Q1}$ should be added and the result should be multiplied by six.

LOSS MODELING FOR DIODES

CONDUCTION LOSSES:

Conduction losses of diode D_4 are given by

$$P_{cond,D4} = I_{D4,av} \cdot V_D + I^2_{D4,rms} \cdot R_D \,. \qquad (11)$$

The expression to find $I_{D4,rms}$ is the same as the expression to find $I_{Q1,rms}$ except for the duty ratio. D_4

conducts when the current is positive and Q_1 is off; therefore the duty ratio for D_4 is $1-D_n=\frac{1}{2}\left(1-M\sin\theta_n\right)$.

Then, $I_{D4,rms}=I\sqrt{\frac{1}{8}-\frac{1}{3\pi}M\cos\phi}$. (12)

The average diode current can be found by averaging as follows:

$$I_{D4,av}=I\left(\frac{1}{2\pi}-\frac{M\cos\phi}{8}\right). \quad (13)$$

Thus

$$P_{cond,D4}=I^2\cdot R_D\cdot\left(\frac{1}{8}-\frac{1}{3\pi}M\cos\phi\right)+I\cdot V_D\cdot\left(\frac{1}{2\pi}-\frac{1}{8}M\cos\phi\right). \quad (14)$$

Figure 5 shows the comparison of the conduction losses of Si and SiC diodes for different *M* and *I* values. Note that V_D and I_D values are obtained from the piece-wise linear (PWL) model of the diodes extracted from experimental results. It is observed that SiC conduction losses are less than Si conduction losses for any *M* and *I*.

SWITCHING LOSSES:

The most important part of the diode switching losses is the reverse recovery losses. The rest of the losses are negligible. Reverse recovery losses will be calculated using the linearized turn-off waveforms in Figure 6.

Average loss in a switching period, T_c, is

$$p_{D4}=\frac{1}{T_c}\int_0^{T_c}v_{sw}i_{sw}\,dt=f_c\frac{V_RI_Rt_b}{2}. \quad (15)$$

I_R can be calculated as follows:

$$I_R=\frac{dI_F}{dt}t_a=\frac{dI_F}{dt}\frac{1}{S+1}t_{rr} \quad (16)$$

where $S\equiv\frac{t_b}{t_a}$.

Then,

$$p_{D4}=\frac{f_cV_R}{2S}\left(\frac{dI_F}{dt}\right)\left(\frac{S\cdot t_{rr}}{S+1}\right)^2. \quad (17)$$

The variables S and t_{rr} in (17) are relatively independent of I_F, and (dI_F/dt) does not depend on I_F, either. The value of (dI_F/dt) is circuit dependent: $(dI_F/dt)=E/L$. Thus, the average D_4 switching loss in an output period, T_o, is

$$P_{sw,D4}=\frac{f_cV_R}{2S}\left(\frac{dI_F}{dt}\right)\left(\frac{S\cdot t_{rr}}{S+1}\right)^2. \quad (18)$$

The diode reverse recovery current also contributes to the average Q_1 conduction losses. This contribution can be calculated by averaging the reverse recovery current in the switching period:

$$i_{D4\to Q1,rms}=\left(\frac{dI_F}{dt}\right)\frac{t_{rr}}{S+1}\sqrt{\frac{t_{rr}}{3T_c}} \quad (19)$$

Thus, the conduction loss contributed to Q_1 by D_4 is

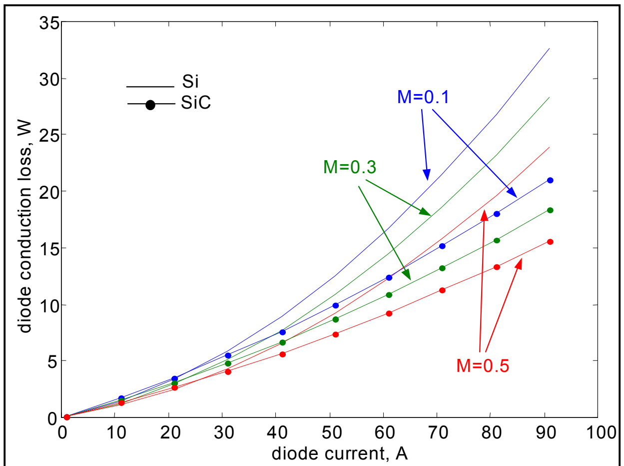

Figure 5. Si and SiC Diode conduction loss with respect to *M* and *I*.

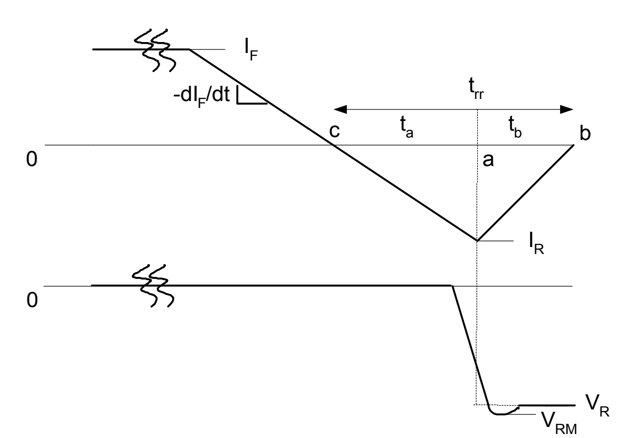

Figure 6. Typical diode turn-off waveform.

$$P_{cond,D4\to Q1} = i^2_{D4-Q1,rms} R_{DS,on} = \frac{t_{rr}}{3T_c}\left[\left(\frac{dI_F}{dt}\right)\frac{t_{rr}}{S+1}\right]^2 R_{DS,on} \quad (20)$$

Figure 2 shows the experimental turn-off waveforms of Si and SiC diodes. The amount of energy loss in the the Si diode turn-off is 3-4 times more than that in the SiC diode. Figure 7 shows the peak reverse recovery current of the Si and SiC diodes. In this figure, it can be observed that as the load increases, the reverse recovery current peak of the Si diode increases while it stays the same in the SiC case. Figure 7 also shows that the reverse recovery current is almost independent of temperature for SiC whereas in Si the current increases dramatically as temperature increases.

SYSTEM LEVEL RESULTS

An HEV traction drive was simulated over the FUDS cycle using ADVISOR. As a result of this simulation, motor torque and speed profiles sampled at 1 Hz were obtained. From these profiles, current peak, *I,* and modulation index, *M,* profiles were calculated assuming V/Hz control.

Using *I* and *M* values, the device power losses are calculated using (7), (10), (14), (18), and (20). Figure 8a shows a comparison of Si and SiC diode losses. SiC diodes do not have much of a reverse recovery current; therefore, their switching losses are low. The conduction losses are also low because of SiC properties. This is why SiC diode total losses are lower than those of the Si diode losses in the inverter. Figure 8b, on the other hand, shows the total MOSFET losses. Although the switching losses of Si and SiC MOSFETs are similar, the big difference between their total losses is due to the conduction losses. The specific on-resistance for the SiC MOSFET is 0.3×10^{-3} Ω-cm^2; for the Si MOSFET, it is 180×10^{-3} Ω-cm^2.

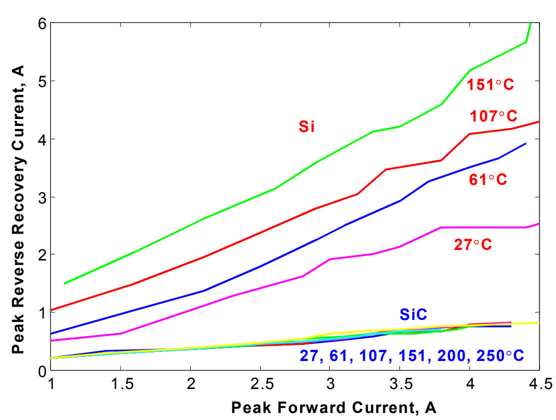

Figure 7. Experimental Si and SiC peak reverse recovery peak current values at different temperatures.

Figure 9a shows the total device losses of the three-phase inverter. As can be seen from the figure, the Si inverter has high losses compared with those of the SiC inverter. Corresponding energy loss in the Si inverter is 925 W·s and in the SiC inverter is 338 W·s over the FUDS cycle. With lower device losses, the SiC inverter is expected to have a higher efficiency. Figures. 9b and 9c show the motoring efficiency of the inverter. It is around 90-95% for the SiC inverter, while it is only 80-85% for the Si inverter. (Note that the zero efficiency points correspond to the instants where the motor is stopped or generating and there is no positive power flow through the inverter.). Higher efficiency also results in less need for recharging the battery.

The junction temperature profiles of the MOSFETs are calculated by feeding the loss profiles to the device thermal equivalent circuit. For this example, the junction temperature profiles can be seen in Figure 10. The

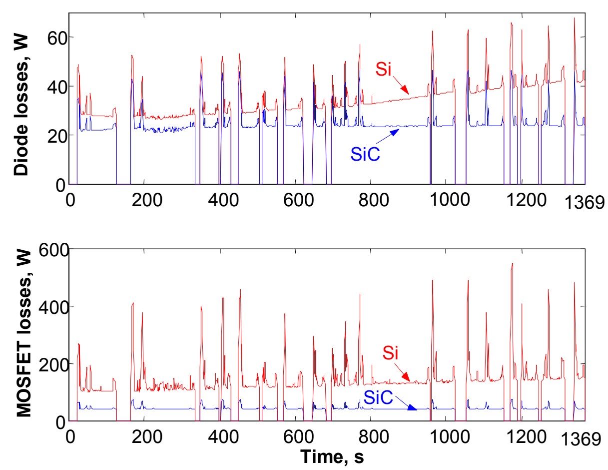

Figure 8. Total losses of each MOSFET and diode over the FUDS cycle (Si-red, top, and 4H-SiC-blue).

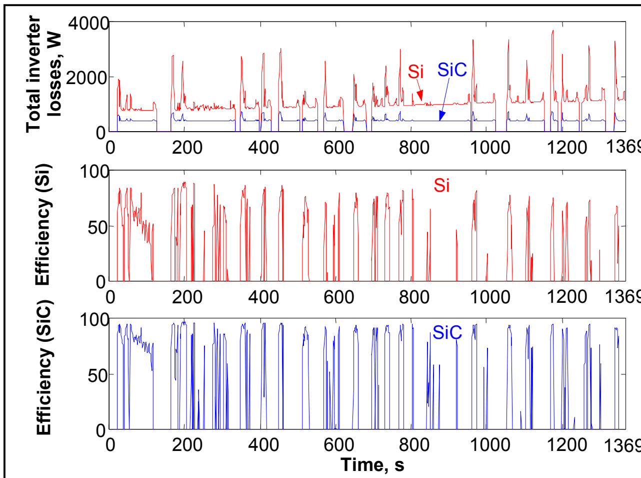

Figure 9. Total losses and the efficiency of the inverter over the FUDS cycle (Si-red, top, and 4H-SiC-blue).

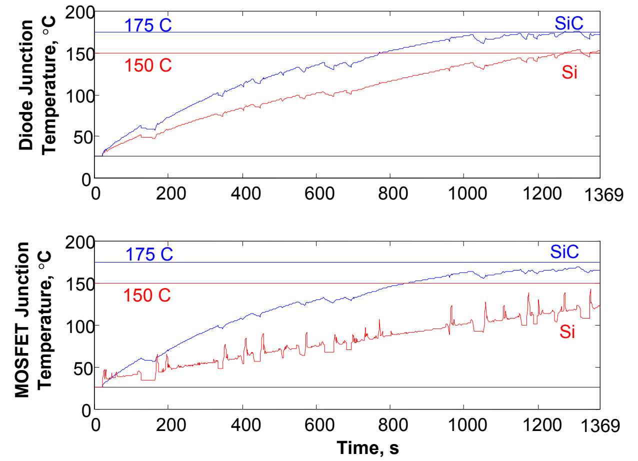

Figure 10. Junction temperature profiles of a Si MOSFET and a SiC MOSFET in the three-phase inverter with heatsink (Si-red, bottom, and 4H-SiC-blue, top two).

heatsinks for the MOSFETs are chosen to limit the junction temperature to the rated values: 150°C for Si and 175°C (Infineon datasheet) [6] for SiC. Theoretically, SiC devices can withstand higher temperatures. Normally, for the kind of inverter discussed in this paper, water-cooled heatsinks are used. However, for ease of calculation, natural air-cooled aluminum-finned heatsinks are considered here. For the whole inverter, six diodes and six MOSFETs should be taken into consideration. Table I shows the volume and weight of the heatsinks needed for the diodes, MOSFETs, and whole inverter. Using SiC power devices, 1392 cm^3 of volume and 3.75 kg of weight are saved (Table I). The savings will be greater when the high-temperature device packaging issues are solved and SiC power devices rated for higher temperatures are commercially available.

In an HEV, size is extremely important because the amount of space available is limited. The weight reduction and efficiency increase result in an increase in the fuel economy of the vehicle.

CONCLUSIONS

1. SiC devices are expected to dominate Si devices in the near future for transportation applications because of their superior qualities.
2. An experimentally validated model for Si and SiC diodes has been developed and presented in this paper. The model helps to evaluate the system-level effects of using SiC diodes for HEV applications.
3. The model has shown that a significant reduction in power electronics converter conduction and switching losses can be achieved by replacing Si devices with those made from SiC. This change means a much-reduced thermal management system is possible in the vehicle, with system benefits such as a reduction in the weight, volume, and cost of converter heat sink requirements.

Table I. Heatsink mass and volume for each device and inverter

	Volume (cm^3)	Mass (g)
Si diodes	444	1200
SiC diodes	162	450
Si MOSFETs	1554	4200
SiC MOSFETs	444	1200
Si inverter	***1998***	***5400***
SiC inverter	***606***	***1650***

CONTACTS

Leon M. Tolbert received the B.E.E., M.S., and Ph.D. degrees in electrical engineering from the Georgia Institute of Technology. He joined the Engineering Division of Lockheed Martin Energy Systems in 1991 and worked on several electrical distribution and power quality projects at the three U.S. Department of Energy plants in Oak Ridge, Tennessee. In 1997, he became a Research Engineer in the Power Electronics and Electric Machinery Research Center (PEEMRC) at the Oak Ridge National Laboratory (ORNL). He was appointed as an assistant professor in the Department of Electrical and Computer Engineering at The University of Tennessee (UT) in Knoxville in 1999. He is also a participating faculty member of the Graduate Automotive Technology Education (GATE) Center at UT. He is an adjunct participant at ORNL and conducts joint research at the National Transportation Research Center (NTRC). Leon's e-mail address is tolbert@utk.edu.

Burak Ozpineci received a B.S. in electrical engineering from the Middle East Technical University, Turkey, and a M.S. in electrical engineering from The University of Tennessee. He joined the Post-Masters Program with the Power Electronics and Electric Machinery Research Center at the Oak Ridge National Laboratory in 2001, and he currently is a Ph.D. student in Electrical and Computer Engineering at The University of Tennessee. His research interests include soft-switching inverters and silicon carbide-based power electronic circuits. Burak's e-mail address is ozpineci@utk.edu.

Syed K. Islam received the M.S., and Ph.D. degrees in electrical engineering from the University of Connecticut in 1987 and 1994, respectively. From January 1994 through July 1994, he worked as an ASIC Design Engineer in Transwitch Corporation. He was an assistant professor at the University of North Florida from 1994 to 1999. Since August 1999, he has been the John W. Fisher Professor in the Department of Electrical and Computer Engineering at The University of Tennessee (UT) in Knoxville. At UT, he is the faculty coordinator for the "University of Tennessee/Oak Ridge National Laboratory Joint Program in Mixed-Signal VLSI and Monolithic Sensors". He is also affiliated with the Microelectronic/Optoelectronic Research Laboratory at the University of Connecticut and the Center of

Environmental Biotechnology at UT. Syed's e-mail is sislam@utk.edu

Fang Zheng Peng received the B.S. degree from Wuhan University, Wuhan, China, and the M.S. and Ph.D. degrees from Nagaoka University of Technology, Japan, in 1983, 1987, and 1990, respectively, all in electrical engineering. From 1990 to 1992, he was a Research Scientist with Toyo Electric Manufacturing Company, Ltd., where he was engaged in research and development of active power filters, flexible ac transmission systems (FACTS) applications, and motor drives. From 1992 to 1994, he was a Research Assistant Professor at Tokyo Institute of Technology, where he initiated a multilevel inverter program for FACTS applications and a speed-sensorless vector control project. From 1994 to 1997, he was a Research Assistant Professor at the University of Tennessee, working for Oak Ridge National Laboratory (ORNL). From 1997 to 2000, he was a Senior Staff Member at ORNL and Lead (principal) Scientist of the Power Electronics and Electric Machinery Research Center. In 2000, he joined Michigan State University in East Lansing, as an Associate Professor. Fang's e-mail is fzpeng@egr.msu.edu

REFERENCES

1. M. Bhatnagar and B. J. Baliga, "Comparison of 6H-SiC, 3C-SiC, and Si for power devices," *IEEE Trans. on Electron Devices*, 40 (3), pp. 645-655, March 1993.
2. K. Shenai, R. S. Scott, B. J. Baliga, "Optimum semiconductors for high-power electronics," *IEEE Transactions on Electron Devices*, 43(9), pp. 1811-1823, Sept. 1989.
3. A Elasser, M. Kheraluwala, M. Ghezzo, R. Steigerwald, N. Krishnamurthy, J. Kretchmer, and T. P. Chow, "A comparative evaluation of new silicon carbide diodes and state-of-the-art silicon diodes for power electronic applications," *IEEE IAS Annual Meeting Conference Proceedings*, pp. 341-345, 1999.
4. B. Ozpineci, L. M. Tolbert, S. K. Islam, M. Hasanuzzaman, "Effects of silicon carbide (SiC) power devices on HEV PWM inverter losses", *The Annual Conference of the IEEE Industrial Electronics Society (IECON'01)*, pp. 1187-1192, 2001.
5. Q. Huang and B. Zhang, "Comparing SiC switching power devices: MOSFET, NPN transistor and GTO transistor," *Solid State Electronics*, Pergamon Press, pp. 325-340, 2000.
6. http://www.infineon.com/cgi/ecrm.dll/ecrm/scripts/prod_cat.jsp?oid=-8681
7. N. Mohan, T. M. Undeland, W. P. Robbins, *Power Electronics*, 2nd Edition, John Wiley & Sons, New York, 1995.
8. D. Schroeder, *Semiconductor Material and Device Characterization*, John Wiley & Sons, New York, 1990.
9. C.M. Johnson, N.G. Wright, S. Ortolland, D. Morrison, K. Adachi, A. O'Neill, "Silicon carbide power devices: hopeful or hopeless?", *IEE Colloquium on Recent Advances in Power Devices*, pp. 10/1 -10/5, 1999.
10. R. Ragunathan, D. Alok, B.J. Baliga, " High Voltage 4H-SiC Schottky Diodes", *IEEE Electron Device Letters*, 16(6), pp. 226-227, June 1995.
11. Itoh, T. Kimoto, H. Matsunami, "High performance of high-voltage 4H-SiC Schottky barrier diodes", *IEEE Electron Device Letter*, 16(6), pp. 280-282, June 1995.
12. W. Wright, J. Carter, P. Alexandrov, M. Pan, M. Weiner, J.H. Zhao, "Comparison of Si and SiC diodes during operation in three-phase inverter driving an AC induction motor", *IEE Electronics Letters*, 37(12), June 2001.
13. J.B. Dufrene, G. Carter, J.B. Casady, I. Sankin, D.C. Sheridan, W. Draper, M. Mazzola, "High-voltage (600 to 3 kV) silicon carbide diode development", *IEEE APEC 2001*, pp. 1253-1257, Anaheim, 2001.
14. A.R. Hefner, Jr., R. Singh, Jih-Sheng Lai, D.W. Berning, S. Bouche, C. Chapuy, "SiC power diodes provide breakthrough performance for a wide range of applications", *IEEE Transactions on Power Electronics*, 16(2) , pp. 273–280, March 2001.
15. A.R. Hefner, D. Berning, J. S. Lai, C. Liu, R. Singh, T. Kamgaing, J. Bernstein, "Silicon carbide merged PiN schottky diode switching characteristics and evaluation for power supply applications," *IEEE IAS Annual Meeting Conf Proc.*, pp. 2948-2954, 2000.
16. K. Berringer, J. Marvin, P. Perruchoud, "Semiconductor power losses in ac inverters," *IEEE IAS Annual Meeting Conf Proc.*, pp. 882-888, 1995.

ACRONYMS

ADVISOR – ADvanced VehIcle SimulatOR

EMI – Electromagnetic Interference

FUDS – Federal Urban Driving Schedule

HEV – Hybrid Electric Vehicle

MOSFET - Metal Oxide Semiconductor Field Effect Transistor

ORNL – Oak Ridge National Laboratory

PWM – Pulse Width Modulation

PWL – Piecewise Linear

Si – Silicon

SiC – Silicon Carbide

NOMENCLATURE

g_m	= transconductance of the MOSFET (Ω^{-1})
BV	= breakdown voltage (V)
E_c	= avalanche breakdown electric field (V/cm)
J'	= peak drain current density (A/cm^2)
V	= applied voltage (V)
V_{GH}, V_{GL}	= Highest and lowest applied gate voltages of the MOSFET (V)
V_{th}	= threshold voltage of the MOSFET (V)
ε_s	= permittivity of the semiconductor (F/cm)
$R_{Ds,on}$	= on resistance of the MOSFET (Ω)
I	= peak drain current (A)
M	= modulation index
ϕ	= current phase angle (radians)
I_R	= peak reverse recovery current of the diode (A)
V_R	= reverse voltage applied to the diode (V)
R_D	= on resistance of the diode
V_D	= voltage drop of the diode
t_{rr}	= total reverse recovery time (s)
t_a, t_b	= defined in Fig. 6
S	= snappiness factor t_b/t_a
A	= chip area (cm^2)
f_o, T_o	= output voltage frequency and period
f_c, T_c	= switching frequency and period
T_e	= torque developed by the electric machine
ω_r	= mechanical speed of the electric machine
η	= efficiency of the electric machine
p	= number of poles of the electric machine